Pseudo Youla-Kucera Parameterization with Control of the Waterbed Effect for Local Loop Shaping

Xu Chen[*][a], Tianyu Jiang[a], Masayoshi Tomizuka[b]

[a]Department of Mechanical Engineering, University of Connecticut, Storrs, CT, 06269, USA.

[b]Department of Mechanical Engineering, University of California, Berkeley, CA, 94720, USA.

Abstract

This paper discusses a discrete-time loop shaping algorithm for servo enhancement at multiple wide frequency bands. Such design considerations are motivated by a large class of practical control problems such as vibration rejection, active noise control, and periodical reference tracking; as well as recent novel challenges that demand new design in the servo technologies. A pseudo Youla-Kucera parameterization scheme is proposed using the inverse system model to bring enhanced control at selected local frequency regions. Design methodologies are created to control the waterbed amplifications that come from the fundamental limitations of feedback control. Finally, simulation and experimental verification are conducted in precision control and semiconductor manufacturing.

Key words: digital control, vibration rejection, loop shaping, active noise control, Youla-Kucera parameterization

1 Introduction

Recent technology innovations are urging the penetration of customized controls in modern precision systems and advanced manufacturing. For instance, in 2011, the wafer scanning process in semiconductor manufacturing requires a control precision which can be mimicked by repetitively driving on a highway segment, under *mm* scale error tolerance between consecutive iterations. In the disk drive industry, new external disturbances—such as vibrations from high-power audio speakers and adjacent drives (in data center and cloud storage)—have become the most important source of the position error in data reading and writing [1]. Both examples demand a control precision at nm scale, with extremely low sensitivity against vibrations and noises.

To reach the required servo goals, enhanced control at selected frequency (or frequency ranges) has been recognized to be essential in many fields including precision mechatronics [2], active suspensions [3], cooling systems [4], and the aforementioned semiconductor manufacturing [5] and information storage systems [6]. Based on

how the enhancements are placed, control algorithms have been proposed to cover: (i) integer multiples of a fundamental frequency, using repetitive control and its variants [7,8,9,10]; (ii) nonrestrictive multiple frequencies, via peak filters [11], adaptive feedforward cancellation [12], disturbance observers [13,6], and internal-model-principle based Youla-Kucera parameterization [14,15,16,17,3]; (iii) broadband frequencies, based on, e.g., adaptive variance minimization [18], and sensor-based adaptive noise cancellation [19]. From the viewpoint of shaping the response of the servo loop, such *local loop shaping* (LLS) algorithms can be classified into: (i) shaping of the open-loop frequency response [11]; (ii) design based on internal model principle and/or time-domain cancellations [9,12,14,15,16,17,6]; (iii) direct shaping of the sensitivity function [18,13,3].

A major recognition from the LLS literature is the significant challenge raised from Bode's Integral Theorem, which guarantees (under mild assumptions that are commonly satisfied in practice) the occurrence of error amplifications during loop shaping. Such "waterbed" limitation—particularly important for LLS at *multiple* frequency locations—has attracted great research attention, and recently been extensively investigated in a benchmark on adaptive narrow-band vibration rejection [3]. Evolving from earlier design of "achieving enhanced local servo performance while maintaining the system

[*] Tel. +1-860-486-3688.

Email addresses: xchen@engr.uconn.edu (Xu Chen[*]), tianyu.jiang@uconn.edu (Tianyu Jiang), tomizuka@me.berkeley.edu (Masayoshi Tomizuka).

stability," more and more algorithms are emerging with the philosophy of achieving LLS with bounded waterbed effect. Examples in the area of narrow-band LLS include [17,3,13,10,6]. Based on the results, infinite-impulse-response (IIR) filters are being more and more adopted over the conventional choice of finite-impulse-response (FIR) filters for waterbed mitigation.

Many novel applications, including the two examples at the beginning of this section, demand enhanced servo at not only single frequencies but also wide frequency bands. Motivated by the aforementioned theoretical challenges in conjunction with the rise of new applications that place more stringent performance requirements, this paper provides a pseudo Youla-Kucera (YK) parameterization scheme for narrow- and wide-band LLS. Several theoretical limits of performance are identified, which explains the difference and fundamental challenge of wide-band LLS compared with its narrow-band analogue. Using a robust pseudo version of YK parameterization—a formulation of all stabilizing controllers—we construct an LLS scheme and discuss its design flexibility and intuitions. A particular contribution of the paper is a systematic design methodology to control the fundamental waterbed constraint in LLS. We show that with an add-on pole/zero modulation in the inverse-based YK scheme, error amplifications in LLS can be flexibly controlled over the frequency domain, to accommodate different servo requirements and disturbance spectra.

The proposed algorithm focuses on obtaining an analytic LLS solution of the central Q filter in YK parameterization, instead of an optimal implicit one, from e.g. weighted sensitivity minimization via optimization and H_∞ theories. Different from conventional servo problems, LLS highly depends on the specific disturbance profiles, which can vary among systems and even change with respect to time. The solution approach in the present paper is made for more convenient incorporation of features such as adaptive control (to attenuate unknown or time-varying disturbance spectra), and industrial tuning (where a direct controller parameterization can be easier for implementation across different product platforms).

Notations: We focus on controlling single-input single-output (SISO) systems. Throughout the paper, the calligraphic $\mathcal{S}$ and $\mathcal{R}$ denote, respectively, the set of *stable proper rational transfer functions*; and the set of *proper rational transfer functions*. When a linear time invariant (LTI) plant P is stabilized by an LTI controller C (in a negative feedback loop), $S(\triangleq 1/(1 + PC))$ and $T(\triangleq PC/(1 + PC))$ denote, respectively, the sensitivity[1] and the complementary sensitivity functions. Fi-

nally, if $n = 0$, then $\sum_{i=1}^{n} a_i = 0$ and $\prod_{i=1}^{n} a_i = 1$.

2 Review of YK Parameterization

Let $G \in \mathcal{R}$. (N, D) is called a coprime factorization of G over $\mathcal{S}$ if: (i) $G = ND^{-1}$, (ii) $N(\in \mathcal{S})$ and $D(\in \mathcal{S})$ are coprime transfer functions, and (iii) $D^{-1} \in \mathcal{R}$.

Theorem 1 (YK parameterization) *[20,21] If a SISO plant $P = N/D$ can be stabilized by a negative-feedback controller $C = X/Y$, with (N, D) and (X, Y) being coprime factorizations over $\mathcal{S}$, then any stabilizing feedback controller of P can be parameterized as*[2]

$$C_{all} = \frac{X + DQ}{Y - NQ} : \ Q \in \mathcal{S}, \ Y(\infty) - N(\infty)Q(\infty) \neq 0 \quad (1)$$

Remark 1 *YK parameterization advantageously changes the principle of feedback design by rendering the new sensitivity function to:*

$$\tilde{S} = \frac{1}{1 + PC_{all}} = \frac{1}{1 + PC}\left[1 - \frac{N}{Y}Q\right] \quad (2)$$

Literature often additionally normalizes the coprime factorization, such that $NX + DY = 1$ and thus $\tilde{S} = D(Y - NQ)$. For LLS which is commonly conducted upon an existing closed loop that operates under regular servo performance, we keep the structure of (2), and interpret Theorem 1 as an add-on scheme that decouples S to the product of the baseline sensitivity $1/(1 + PC)$ and the add-on affine module $1 - NQ/Y$.

3 LLS with Discrete-time Pseudo YK Design

We discuss first a special discrete-time case of Theorem 1 and its generalization for LLS, then provide the corresponding design of Q and control of the waterbed.

Proposition 2 *Consider a stable discrete-time negative feedback loop consisting of a controller $C(z)$, and a plant $P(z)$ whose relative degree is m. If $P^{-1}(z)$ and $C(z)$ are stable, then*

$$C_{all}(z) = \frac{C(z) + z^{-m}P^{-1}(z)Q(z)}{1 - z^{-m}Q(z)}, \ Q(z) \in \mathcal{S} \quad (3)$$

parameterizes all stabilizing controllers for $P(z)$, and the sensitivity function is

$$S(z) = \frac{1 - z^{-m}Q(z)}{1 + P(z)C(z)} \triangleq S_o(z)\left(1 - z^{-m}Q(z)\right) \quad (4)$$

Proof follows by letting $X(z) = C(z)$, $Y(z) = 1$, $N(z) = z^{-m}$, and $D(z) = z^{-m}P^{-1}(z)$ in Theorem 1.

Proposition 2 reduces the add-on module in the sensitivity function to $1 - z^{-m}Q(z)$ in (4). The inverse-based parameterization has made the added module simple and depend little on $C(z)$ and $P(z)$ (only the delay z^{-m} appears here). This was achieved by confining to plants with stable inverses, and closed loops with stable baseline controllers. These two conditions are relaxed in a *pseudo* YK scheme in the next result.

Proposition 3 *Consider a stable discrete-time negative feedback loop consisting of a controller $C(z)$, and a plant $P(z)$ whose relative degree is m. Let*

$$\tilde{C}(z) = \frac{C(z) + z^{-m}\hat{P}^{-1}(z)Q(z)}{1 - z^{-m}Q(z)}, \ Q(z) \in \mathcal{S} \quad (5)$$

where $\hat{P}^{-1}(z)$ is chosen stable. If $P(z) = \hat{P}(z)$, then the new feedback loop consisting of $P(z)$ and $\tilde{C}(z)$ has guaranteed stability. Otherwise, the new feedback loop is stable if the roots of the following characteristic equation are all inside the unit circle:

$$z^m A_Q(z)B_{\hat{P}}(z)[A_C(z)A_P(z) + B_C(z)B_P(z)] \\ + A_C(z)B_Q(z)[A_{\hat{P}}(z)B_P(z) - A_P(z)B_{\hat{P}}(z)] = 0 \quad (6)$$

where $B_G(z)$ and $A_G(z)$ denote the coprime numerator and denominator polynomials of a transfer function G.

Proof With $P(z) = B_P(z)/A_P(z), C(z) = B_C(z)/A_C(z)$, $\hat{P}(z) = B_{\hat{P}}(z)/A_{\hat{P}}(z)$, and $Q(z) = B_Q(z)/A_Q(z)$, (5) transforms to

$$\tilde{C}(z) = \frac{A_Q(z)B_{\hat{P}}(z)B_C(z) + z^{-m}A_C(z)A_{\hat{P}}(z)B_Q(z)}{B_{\hat{P}}(z)A_C(z)[A_Q(z) - z^{-m}B_Q(z)]} \quad (7)$$

With (7), the closed-loop characteristic equation is (6). The root condition in the second half of the proposition then readily follows. If $P(z) = \hat{P}(z)$, (6) reduces to

$$A_Q(z)B_{\hat{P}}(z)[A_C(z)A_P(z) + B_C(z)B_P(z)] = 0 \quad (8)$$

Hence the closed-loop poles are composed of the baseline closed-loop poles and the poles of $Q(z)$ and $\hat{P}^{-1}(z)$. As the baseline feedback loop, $Q(z)$, and $\hat{P}^{-1}(z)$ are all stable, the new closed loop is thus stable. □

Proposition 3 relaxes the requirements on stable C and P^{-1} by focusing on LLS and dropping the attempt to parameterize all the stabilizing controllers. More specifically, the subclass of all stabilizing controllers (5) can be seen to always retain the unstable poles (which can occur for stabilizing certain unstable plants) of C, if any. On the other hand, from the viewpoint of implementation, a perfect plant model is unrealistic in practice (due to high complexities or system uncertainties). In this sense, a practical YK parameterization has to be an approximation, or a robust version, of the ideal cases in

Section 2 and Proposition 2. As a perfect plant model is not available anyway, a *stable* nominal inversion $\hat{P}^{-1}(z)$ is adopted in Proposition 3. This is one constraint that is achievable in a large class of practical systems. [3] Moreover, the next two paragraphs will show that the mismatch between $\hat{P}^{-1}$ and P^{-1}, if any, can actually be allowed in the frequency regions that do not require servo enhancement in LLS.

With (5), the sensitivity function $1/(1 + P(z)\tilde{C}(z))$ is

$$S(z) = \frac{1 - z^{-m}Q(z)}{1 + P(z)C(z) + z^{-m}Q(z)(\hat{P}^{-1}(z)P(z) - 1)} \quad (9)$$

If $\hat{P}^{-1}(e^{j\omega})P(e^{j\omega}) = 1$, namely, at frequencies where the inverse model is accurate, (9) gives

$$S(e^{j\omega}) = \frac{1 - e^{-mj\omega}Q(e^{j\omega})}{1 + P(e^{j\omega})C(e^{j\omega})} \quad (10)$$

i.e. the decoupling of sensitivity in (4) remains valid in the frequency domain. Enhancing the closed-loop performance at ω_i thus translates to designing $e^{-mj\omega_i}Q(e^{j\omega_i}) = 1$, which gives perfect disturbance rejection ($S(e^{j\omega_i}) = 0$) and reference tracking ($T(e^{j\omega_i}) = 1$) at ω_i. Meanwhile, at ω_k where there are large model uncertainty and mismatches, high-performance control intrinsically has to be sacrificed for robustness based on robust control theory. We will thus make $Q(e^{j\omega_k}) \approx 0$, to keep the influence of the mismatch element $z^{-m}Q(z)(\hat{P}^{-1}(z)P(z) - 1)$ small in (9). More formally, as $Q(z)$ and the baseline sensitivity $1/(1 + P(z)C(z))$ are both stable, if $|Q(e^{j\omega})(P(e^{j\omega})\hat{P}^{-1}(e^{j\omega}) - 1)| < |1 + P(e^{j\omega})C(e^{j\omega})|$ in (9) $\forall \omega$, $S(z)$ will have guaranteed stability.

Fig. 1 presents a realization of the pseudo YK scheme. By block diagram analysis, one can show that when $r(k) = 0$ and $z^{-m}Q(z)|_{z=e^{j\omega_i}} \approx 1$, $c(k)$ approximates $-d(k)$ at ω_i (hence canceling the disturbance). Such time-domain intuition can be used for tuning during implementations.
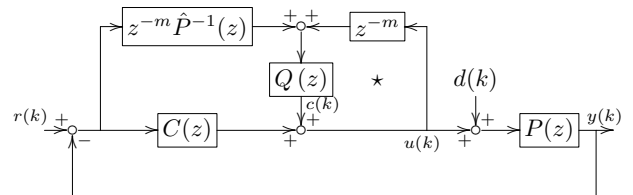

Fig. 1. Block diagram of pseudo YK parameterization

---

[3] Indeed, inverse-based design has long been used in motion control, e.g., in feedforward designs.

Next we provide solutions of Q for LLS, and then several design tools to control the waterbed.

Prototype LLS Solution *Let $\{\omega_i\}_{i=1}^n$ be a set of distinct frequencies (in rad). Let $A_\zeta(z) = \prod_{i=1}^n(1 - 2\zeta\cos\omega_i z^{-1} + \zeta^2 z^{-2})$—or after multiplication—$A_\zeta(z) = 1 + a_1\zeta z^{-1} + \cdots + a_n\zeta^n z^{-n} + \cdots + a_1\zeta^{2n-1}z^{-2n+1} + \zeta^{2n}z^{-2n}$, where $\zeta = \alpha$ or β, $0 < \alpha < \beta \le 1$, and β is very close or equal to 1. Let $P(z)$ be stabilized by (5), with $P(e^{j\omega_i}) = \hat{P}(e^{j\omega_i})$, and*

$$Q(z) = \frac{B_Q(z)}{A_\alpha(z)} : \; K(z)A_\beta(z) + z^{-m}B_Q(z) = A_\alpha(z) \quad (11)$$

where $K(z) = 1$ if $m = 1$; $K(z) = k \in (0,1]$ if $m = 0$; and $K(z)$ is an FIR filter when $m > 1$. Then at each ω_i, a notch is created in the magnitude response of the sensitivity function. Furthermore, if $\beta = 1$, the design achieves perfect disturbance rejection at $\{\omega_i\}_{i=1}^n$ and $Q(e^{j\omega_i}) = e^{jm\omega_i}$.

We verify the solution along with a discussion on several central concepts in LLS. (11) yields

$$1 - z^{-m}Q(z) = \frac{A_\beta(z)}{A_\alpha(z)}K(z) \quad (12)$$

For each ω_i, $A_\beta(z)/A_\alpha(z)$ has a pair of damped pole and zero $(\alpha e^{\pm j\omega_i}, \beta e^{\pm j\omega_i})$. α controls the width of the attenuation range. The zero $\beta e^{j\omega_i}$—on or close to the unit circle—provides small gains to $|1 - e^{-j\omega m}Q(e^{j\omega})|$ when ω is close to ω_i. If $\beta = 1$, applying $\cos(\omega_i) = (e^{-j\omega_i} + e^{j\omega_i})/2$ gives $A_{\beta=1}(e^{j\omega_i}) = (1 - 2\cos\omega_i e^{-j\omega_i} + e^{-2j\omega_i})\prod_{j=1,j\ne i}^n(1 - 2\cos\omega_j e^{-j\omega_i} + e^{-2j\omega_i}) = 0$, and hence $Q(e^{j\omega_i}) = e^{jm\omega_i}$ in (12), which renders $S(e^{j\omega_i}) = 0$ in (10) and therefore full disturbance rejection at ω_i.

$K(z)A_\beta(z) + z^{-m}B_Q(z) = A_\alpha(z)$ in (11) is a Diophantine equation (see, e.g. [22]), and is always solvable using a Sylvester matrix, as $A_\beta(z)$ and z^{-m} are coprime. The minimum-order solution satisfies $B_Q(z) = b_{Q,0} + b_{Q,1}z^{-1} + \cdots + b_{Q,2n-1}z^{-2n+1}$ and

$$K(z) = k_0 + k_1 z^{-1} + \cdots + k_{m-1}z^{-m+1} \quad (13)$$

(if $m = 0$, $K(z) = k$). For low-order problems, $b_{Q,i}$'s and k_i's can be directly obtained by the method of undetermined coefficients.

Example 1 *Let $m = 2$, $\beta = 1$, and $n = 1$. From (13), $K(z) = k_0 + k_1 z^{-1}$. Matching coefficients of z^{-i}'s in the Diophantine equation (11) gives*

$$Q(z) = (\alpha - 1)\frac{(\alpha + 1 - a^2) - az^{-1}}{1 + a\alpha z^{-1} + \alpha^2 z^{-2}} \quad (14)$$

with $a = -2\cos(\omega_1)$ and $K(z) = 1 + (\alpha - 1)az^{-1}$.

Corresponding to the notch shape of $A_\beta(z)/A_\alpha(z)$, $Q(z)$ from (12) is a special bandpass filter (see Example 1 and Fig. 6), which reduces the influence of model mismatch outside the Q-filter passband for enhanced robust stability [recall (9)]. Note, however, that no practical bandpass filters are ideal, especially when the passband gets wider. Along with the desired notch shape, $\max_\omega |1 - z^{-jm\omega}Q(e^{j\omega})|(= \|1 - z^{-m}Q(z)\|_\infty)$ will exhibit the waterbed effect of exceeding 1. The root cause comes from the following fact from fundamental limitations of feedback control.

Corollary 4 *Let $Q(z) \in \mathcal{S}$. Then*

$$\int_0^\pi \ln|1 - e^{-mj\omega}Q(e^{j\omega})|\mathrm{d}\omega = \pi\left(\sum_{i=1}^l \ln|\gamma_i| - \ln|\sigma + 1|\right)$$

where γ_i ($l \ge 0$) are the unstable (outside the unit circle) zeros of $1 - z^{-m}Q(z)$, and $\sigma = \lim_{z\to\infty}\{z^{-m}Q(z)/(1 - z^{-m}Q(z))\}$.

The proof follows by invoking Bode's Integral Theorem [23] and treating $L_Q = z^{-m}Q(z)/(1 - z^{-m}Q(z))$ as the open-loop transfer function in a negative feedback loop. As a particular case, if $m > 0$ and $1 - z^{-m}Q(z)$ has no unstable zeros, then $\int_0^\pi \ln|1 - e^{-mj\omega}Q(e^{j\omega})|\mathrm{d}\omega = 0$.

In Example 1, reducing α increases the LLS bandwidth; however, the zero of $K(z)$ also becomes unstable if $|(\alpha - 1)2\cos\omega_1| > 1$, which increases the sensitivity integral in Corollary 4. Such theoretical challenge of wide-band LLS is seen to match the intuition from the perspective of filter shapes in the paragraph after Example 1.

Remark 2 (Overcoming the waterbed effect) *If $m = 0$, (12) simplifies to $1 - Q(z) = kA_\beta(z)/A_\alpha(z)$. Letting $k \in (0,1)$ gives $Q(\infty) = 1 - k$ and then $\ln|\sigma + 1| = \ln|1/k| > 0$ in Corollary 4. Additionally, $1 - Q$ has no unstable zeros. Hence the Bode's integral is negative. Independent from the baseline design of C, the new sensitivity magnitude can thus be reduced at all frequencies. In common plants, usually $m \ge 1$. For certain non-conventional systems without delays, one observes that LLS design is significantly simplified. In the remainder texts, we focus on the cases with $m \ge 1$.*

Although the overall area integral is constrained by Corollary 4, depending on the disturbance spectrum, performance goals, and robustness of the system in different regions, the waterbed can be controlled via structural designs in $Q(z)$, as shall be discussed next.

3.1 Detuning

One direct approach to reduce the overall waterbed amplification is to design first a regular Q filter in (11) and then detune via $\tilde{Q}(z) = gQ(z)$, $g \in (0,1)$. By reducing $|\tilde{Q}(e^{j\omega})|$, $|1 - e^{-jm\omega}\tilde{Q}(e^{j\omega})|$ is closer to unity outside

the pass bands of $Q(z)$. Mathematically, the next result provides the amount of LLS enhancement under detuning and the reduction of waterbed amplification.

Proposition 5 *Let the plant be stabilized by (5). Let $\beta = 1$; $Q(z)$ be the prototype solution (11); $\tilde{Q}(z) = gQ(z)$, $g \in (0,1)$; and $P(e^{j\omega_i}) = \hat{P}(e^{j\omega_i})$. Then $|S(e^{j\omega_i})| = (1-g)|S_o(e^{j\omega_i})|$ and $||1 - z^{-m}\tilde{Q}(z)||_\infty \leq 1 + g(||1 - z^{-m}\tilde{Q}(z)||_\infty - 1) < ||1 - z^{-m}Q(z)||_\infty$.*

Proof The prototype LLS solution satisfies $Q(e^{j\omega_i}) = e^{jm\omega_i}$. Hence $1 - e^{-jm\omega_i}\tilde{Q}(e^{j\omega_i}) = 1 - g$, and $|S(e^{j\omega_i})| = (1-g)|S_o(e^{j\omega_i})|$ from (10). The second assertion follows from basic properties of H_∞ norm: let Qu denote the output of Q w.r.t. the input signal u, then $||1 - z^{-m}\tilde{Q}||_\infty = \sup_{u \neq 0}\{||[1 - z^{-m}\tilde{Q}]u||_2/||u||_2\} = \sup_{u \neq 0}\{||[1 - z^{-m}gQ]u||_2/||u||_2\} \leq \sup_{u \neq 0}\{||[(1-g)u||_2 + ||g(1 - z^{-m}Q)u||_2]/||u||_2\} = 1 - g + g||1 - z^{-m}Q||_\infty < ||1 - z^{-m}Q||_\infty$, where the last inequality is due to $||1 - z^{-m}Q||_\infty > 1$ from Corollary 4 and $g \in (0,1)$. $\square$

The root reason that detuning relaxes the waterbed effect comes from the fact that unstable zeros of $1 - z^{-m}Q(z)$, if exist, can be pulled into the unit disk by cascading the gain g. From root locus analysis, regard $-z^{-m}gQ(z)$ as the open-loop transfer function, then as g moves from 1 to 0, poles of $1/(1 - gz^{-m}Q(z))$—i.e. zeros of $1 - gz^{-m}Q(z)$—move from poles of $1/(1 - z^{-m}Q(z))$ to poles of $z^{-m}Q(z)$, which are all stable.

Besides the overall detuning to reduce $||1 - z^{-m}Q(z)||_\infty$, $Q(z)$ can be locally manipulated to reduce $|1 - e^{-jm\omega}Q(e^{j\omega})|$ at designer-assigned frequencies. Such localization can be used to build robustness against model mismatch/uncertainties and tackle some particular disturbance spectra. Without loss of generality, we will assume $\beta = 1$ and then apply detuning to control the overall Q-filter gain, if needed.

3.2 Modulation of Zeros

(11) directly embedded the denominator $A_\alpha(z)$ in $Q(z)$. but did not specify the structure of the numerator $B_Q(z)$. One can enforce constrained magnitude by adding fixed zeros such that

$$B_Q(z) = B_0(z)B_Q'(z). \qquad (15)$$

Designing $B_0(z) = 1 - z^{-1}$ for example, will embed a scaled differentiator in $Q(z)$, yielding $Q(e^{j\omega})\big|_{\omega=0} = 0$ (zero DC gain). Fig. 2 presents the effect of such a design, with $\beta = 1$ and $g = 0.8$. The enhanced small gain at low frequency is seen to successfully reduce $|1 - e^{-jm\omega}Q(e^{j\omega})|$ in the highlighted region.
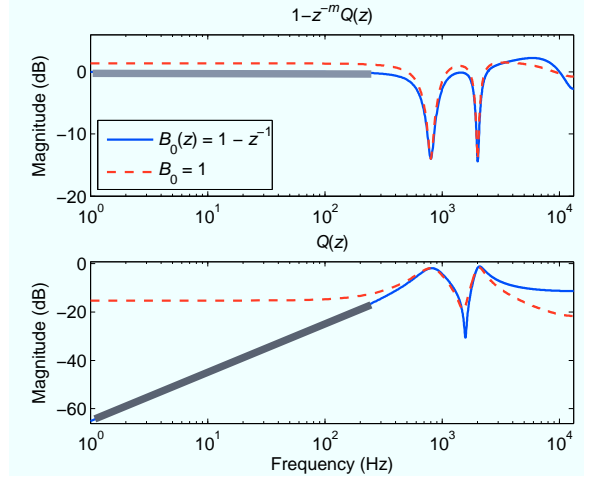

Fig. 2. Effect of a fixed zero at low frequency

Similarly, introducing a fixed zero near $z = -1$ provides enhanced small gains for $Q(z)$ in the high-frequency region. Extending this idea, one can place magnitude constraints at arbitrary desired frequencies, by designing $B_0(z) = 1 - 2\rho\cos\omega_p z^{-1} + \rho^2 z^{-2}$, which places fixed zeros $\rho e^{\pm j\omega_p}$ in (15) to penalize $|Q(e^{j\omega})|$ near ω_p. Combinations can be made, for instance, to form the enhancement in Fig. 3, using $B_0(z) = (1 + 0.7z^{-1})(1 - 0.86z^{-1})(1 - 1.6\cos(2\pi \times 6000T_s)z^{-1} + 0.8^2 z^{-2})(1 - 1.4\cos(2\pi \times 10000T_s)z^{-1} + 0.7^2 z^{-2})$. There, reduced gain is achieved at almost all frequencies outside the pass bands of $Q(z)$.
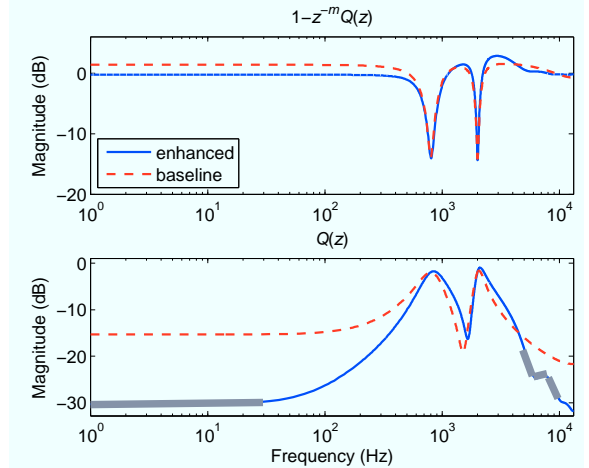

Fig. 3. Effect of combined zeros at different frequencies

With (15), $Q(z)$ is obtained by solving the Diophantine equation $K(z)A_\beta(z) + z^{-m}B_0(z)B_Q'(z) = A_\alpha(z)$. Let the order of $B_0(z)$ be n_{B_0}. If $A_\beta(z)$ and $B_0(z)$ are coprime, the minimum-order solution satisfies $B_Q'(z) = b_{Q,0} + b_{Q,1}z^{-1} + \cdots + b_{Q,2n-1}z^{-2n+1}$; $K(z) = k_0 + k_1 z^{-1} + \cdots + k_{(m+n_{B_0}-1)}z^{-(m+n_{B_0}-1)}$.

Note that the proposed zeros of $B_0(z)$ are all inside the closed unit ball. Unstable zeros in $Q(z)$ raise fundamental limitations on controlling $|1 - e^{-jm\omega}Q(e^{j\omega})|$, as shown next.

Corollary 6 *If $Q(z)(\in \mathcal{S})$ has an unstable zero z_u then*

$$\|1 - z^{-m}Q(z)\|_\infty \geq \prod_{i=1}^{N_p} \frac{|z_u\bar{p}_i - 1|}{|z_u - p_i|} \tag{16}$$

where p_i's are $N_p(\geq 0)$ unstable zeros of $1 - z^{-m}Q(z)$ and $\bar{p}_i$ is the complex conjugate of p_i. If $N_p > 0$, the right hand side of (16) is strictly larger than 1; if $N_p = 0$, the result simplifies to $\|1 - z^{-m}Q(z)\|_\infty \geq 1$.

Proof Applying all-pass factorization such that $1 - z^{-m}Q(z) = M_m(z)\prod_{i=1}^{N_p}(z - p_i)/(z\bar{p}_i - 1)$, where $M_m(z)$ is minimum-phase. Then $\|1 - z^{-m}Q(z)\|_\infty = \|M_m(z)\|_\infty$ and $M_m(z_u)\prod_{i=1}^{N_p}(z_u - p_i)/(z_u\bar{p}_i - 1) = 1$. For $M_m(z)$, $\|M_m(z)\|_\infty \geq |M_m(z_u)|$ by maximum modulus principle. Combining the last three results proves (16). If $N_p = 0$ then $\prod_{i=1}^{N_p}(z - p_i)/(z\bar{p}_i - 1) = 1$. Otherwise straightforward complex analysis gives that $|z_u\bar{p}_i - 1|/|z_u - p_i| > 1$, due to $|z_u| > 1$ and $|p_i| > 1$. $\blacksquare$

3.3 Enhancement by Cascaded IIR Filters

From the frequency-response perspective, cascading two bandpass filters with the same center frequency generates an enhanced one. Consider $Q(z) = Q_0(z)B_0(z)$, where $Q_0(z)$ is the prototype/basic solution from (11) and $B_0(z)$ is a standard bandpass filter with the same center frequencies as $Q_0(z)$. Any standard bandpass design with $B_0(e^{j\omega_i}) = 1$ is applicable here. One candidate choice is

$$B_0(z) = 1 - \eta \frac{A_{\beta=1}(z)}{A_\alpha(z)}, \ \eta \in (0,1] \tag{17}$$

Fig. 4 presents the $Q(z)$ and $1 - z^{-m}Q(z)$ solved from the discussed algorithm. The solid line is the basic solutions from (11) (i.e., $B_0(z) = 1$). Both methods create the required attenuation at around 3000 Hz, while the Q filter with cascaded IIR design has an enhanced bandpass property. Despite a shifted waterbed concentration, the maximum amplification is still around 1.6dB (1.2023) while the attenuation is as large as 50dB (not shown due to limit of figure size) in a wide frequency region.

4 Simulation and Experimental Results

Recall the two examples at the beginning of the Introduction Section. This section provides the experimental verification of the algorithm on one stage of a wafer scanner [10], and the data-in-the-loop simulation on an HDD benchmark [24] using actual audio-vibration test data.
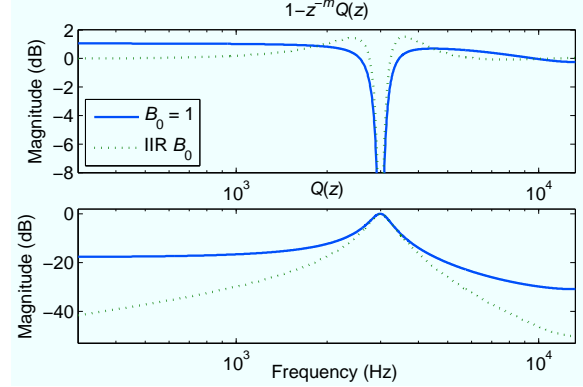

Fig. 4. Effect of cascaded IIR enhancement in $Q(z)$

4.1 Experimental Results on a Wafer-Scanner Testbed

Based on physics, the nominal model of the plant has pure inertia dynamics and satisfies $P_n(z) = 3.129 \times 10^{-7}(z + 1)/[z(z - 1)^2]$ (sampling frequency: 2500 Hz). $P_n(z)$ has a relative degree of two (i.e. $m = 2$), and a
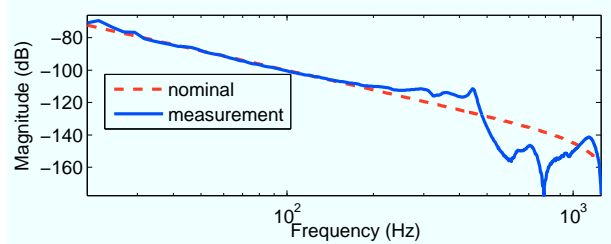

Fig. 5. Plant model of the reticle stage in a wafer scanner

zero on the unit circle. Shifting this zero to be strictly inside the unit circle, and normalizing the gain, we obtain the stable nominal inverse $z^{-m}\hat{P}^{-1}(z) = 10^7/3.47655 \times (z - 1)^2/(z^2 + 0.8z)$. One can verify that $\hat{P}$ and P_n have almost identical frequency response. The dashed line in Fig. 5 shows the frequency response of $\hat{P}(z)$, which matches with the solid line from system identification experiments up to 150 Hz. Fig. 6 shows the frequency responses of different LLS designs at 100 Hz. The IIR enhancement uses $\eta = 0.9$ in (17); the enhancement at 200 Hz and 700 Hz is achieved by fixing $B_0(z) = (1 - 1.7\cos(2\pi T_s \times 200)z^{-1} + 0.85^2z^{-2})(1 - 1.6\cos(2\pi T_s \times 700)z^{-1} + 0.8^2z^{-2})(1 + 0.7z^{-1})$; the remaining designs use the prototype LLS solution.

The measured sensitivity functions in Fig. 7 demonstrate the challenge of wide-band LLS compared to narrow-band loop shaping. Compared to the solid line, which shows no visible waterbed amplification, a large gain increase occurred between 200 Hz and 300 Hz in the dashed line, due to $|Q(e^{j\omega})|$ being not sufficiently small to accommodate the model mismatch beyond 200 Hz.

With the cascaded IIR enhancement, $|Q(e^{j\omega})|$ in the dotted line of Fig. 6 decreases rapidly after 200 Hz. Cor-
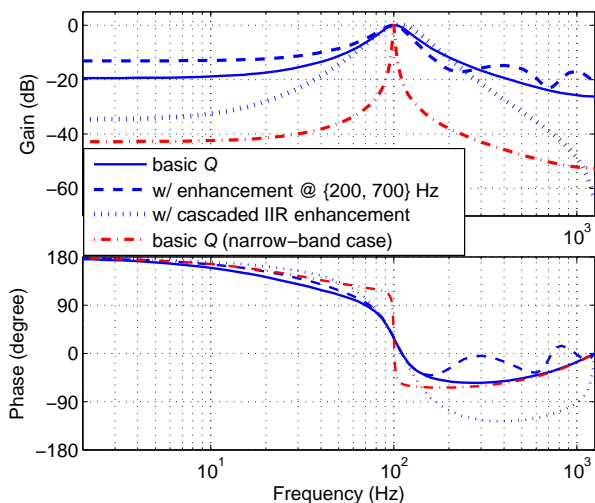
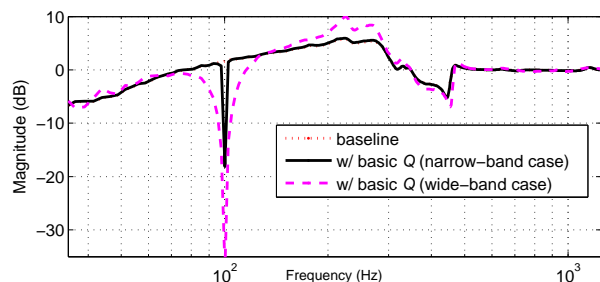Fig. 6. Frequency responses of different Q-filter designs.

Fig. 7. Magnitude response of the sensitivity functions in narrow- and wide-band LLS (only finite gridding of the frequency can be obtained during experiments; both the solid and the dashed lines actually have zero gain at 100 Hz)

respondingly, the large amplification after 200 Hz is removed in the sensitivity function in Fig. 8a. To match the shape of the pass band in Fig. 8, the IIR enhancement yields a larger $|Q(e^{j\omega})|$ between 100 Hz and 200 Hz. This explains the shift of the waterbed effect in the sensitivity function. Applying the zero modulation to reduce $|Q(e^{j\omega})|$ between 100 Hz and 200 Hz (dashed line in Fig. 6), one can remove the amplification below 200 Hz, as shown in Fig. 8.

4.2 Audio-vibration rejection in HDDs

The plant and baseline servo design of the HDD servo benchmark have been described in [24,10]. The top plot of Fig. 9 shows the spectrum of the position error signal (PES) without LLS. After an LLS design that is similar to the dashed line in Fig. 3, the bottom plot of Fig. 9 shows the resulted PES, where the spectrum has been greatly flattened compared to the baseline result. The three-sigma value (sigma is the standard deviation) has reduced from 33.54% TP (Track Pitch) to 22.79% TP (here 1 TP = 254 nm), yielding a 29.07 percent improvement. Notice that 1600 Hz is above the bandwidth of
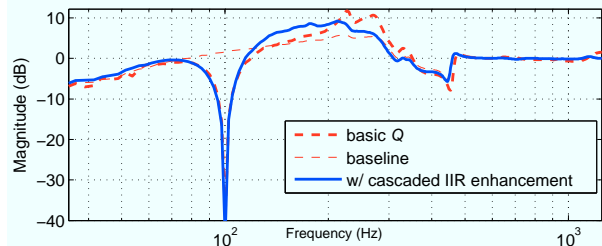
(a) based on IIR enhancement
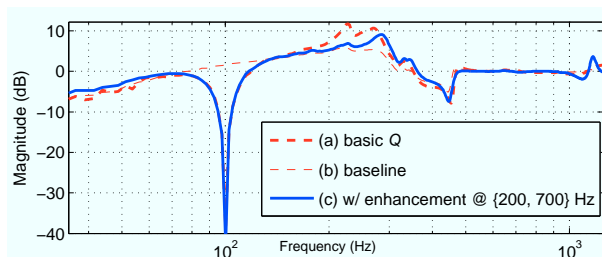
(b) based on zero modulations

Fig. 8. Control of the waterbed effect in wide-band LLS

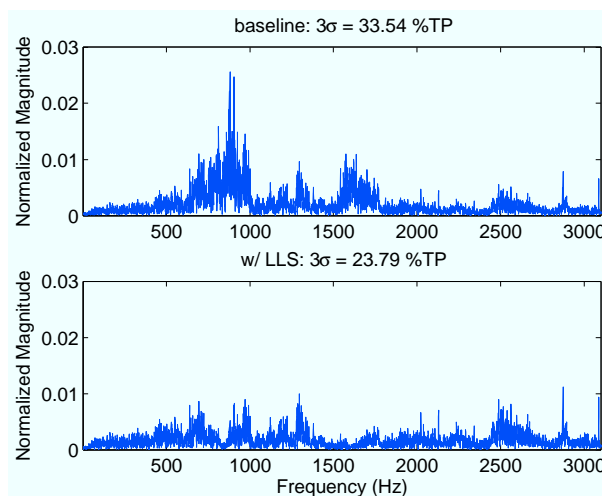the servo system, where disturbance rejection was not feasible in the original baseline design.

Fig. 9. Spectra (FFT) of the PES with and without LLS

5 Conclusions and Discussions

This paper has discussed a pseudo inverse-based Youla-Kucera parameterization scheme for selectively enhancing the closed-loop servo performance at wide frequency ranges. Simulation and experiments have been conducted to validate the proposed designs. In the presence of the fundamental limitation of feedback control, analysis and design methodologies have been presented to control the waterbed effect and minimize the negative impact based on the servo task and the disturbance

spectra. Such design flexibility is particularly needed in precision systems, or applications where the disturbances are composed of rich frequency components.

References

[1] X. Chen, W. Xi, Y. Kim, and K. Tu, "Methods for closed-loop compensation of ultra-high frequency disturbances in hard disk drives and hard disk drives utilizing same," U.S. Patent 8 630 059, January, 2014.

[2] M. Tomizuka, "Dealing with periodic disturbances in controls of mechanical systems," *Annu. Rev. in Control*, vol. 32, no. 2, pp. 193 – 199, 2008.

[3] I. D. Landau, A. C. Silva, T.-B. Airimitoaie, G. Buche, and M. Noe, "Benchmark on adaptive regulation–rejection of unknown/time-varying multiple narrow band disturbances," *European J. Control*, vol. 19, no. 4, pp. 237 – 252, 2013.

[4] R. de Callafon, J. Zeng, and C. E. Kinney, "Active noise control in a forced-air cooling system," *Control Engineering Practice*, vol. 18, no. 9, pp. 1045–1052, Sep. 2010.

[5] T. Oomen, R. van Herpen, S. Quist, M. van de Wal, O. Bosgra, and M. Steinbuch, "Connecting system identification and robust control for next-generation motion control of a wafer stage," *IEEE Trans. Control Syst. Technol.*, vol. 22, no. 1, pp. 102–118, Jan 2014.

[6] X. Chen and M. Tomizuka, "A minimum parameter adaptive approach for rejecting multiple narrow-band disturbances with application to hard disk drives," *IEEE Trans. Control Syst. Technol.*, vol. 20, no. 2, pp. 408 –415, march 2012.

[7] S. Hara, Y. Yamamoto, T. Omata, and M. Nakano, "Repetitive control system: a new type servo system for periodic exogenous signals," *IEEE Trans. Autom. Control*, vol. 33, no. 7, pp. 659 –668, Jul 1988.

[8] M. Tomizuka, T.-C. Tsao, and K.-K. Chew, "Analysis and synthesis of discrete-time repetitive controllers," *ASME J. Dyn. Syst., Meas., Control*, vol. 111, no. 3, pp. 353–358, 1989.

[9] M. Steinbuch, "Repetitive control for systems with uncertain period-time," *Automatica*, vol. 38, no. 12, pp. 2103–2109, 2002.

[10] X. Chen and M. Tomizuka, "New repetitive control with improved steady-state performance and accelerated transient," *IEEE Trans. Control Syst. Technol.*, vol. 22, no. 2, pp. 664–675, March 2014.

[11] L. Sievers and A. von Flotow, "Comparison and extensions of control methods for narrow-band disturbance rejection," *IEEE Trans. Signal Process.*, vol. 40, no. 10, pp. 2377–2391, 1992.

[12] M. Bodson, "Adaptive algorithms for the rejection of sinusoidal disturbances with unknown frequency," *Automatica*, vol. 33, no. 12, pp. 2213–2221, Dec. 1997.

[13] X. Chen and M. Tomizuka, "Selective model inversion and adaptive disturbance observer for time-varying vibration rejection on an active-suspension benchmark," *European J. Control*, vol. 19, no. 4, pp. 300 – 312, 2013.

[14] I. D. Landau, A. Constantinescu, and D. Rey, "Adaptive narrow band disturbance rejection applied to an active suspension–an internal model principle approach," *Automatica*, vol. 41, no. 4, pp. 563–574, Apr. 2005.

[15] Q. Zhang and L. Brown, "Noise analysis of an algorithm for uncertain frequency identification," *IEEE Trans. Autom. Control*, vol. 51, no. 1, pp. 103–110, 2006.

[16] F. Ben-Amara, P. T. Kabamba, and a. G. Ulsoy, "Adaptive sinusoidal disturbance rejection in linear discrete-time systems–part I: Theory," *ASME J. Dyn. Syst., Meas., Control*, vol. 121, no. 4, pp. 648–654, 1999.

[17] Z. Wu and M. Liu, "Adaptive regulation against unknown narrow band disturbances applied to the flying height control in data storage systems," *Asian J. Control*, vol. 16, no. 5, pp. 1532–1540, 2014.

[18] R. A. de Callafon and H. Fang, "Adaptive regulation via weighted robust estimation and automatic controller tuning," *European J. Control*, vol. 19, no. 4, pp. 266 – 278, 2013.

[19] B. Widrow, J. Glover Jr, J. McCool, J. Kaunitz, C. Williams, R. Hearn, J. Zeidler, E. Dong Jr, and R. Goodlin, "Adaptive noise cancelling: principles and applications," *Proc. IEEE*, vol. 63, no. 12, pp. 1692–1716, 1975.

[20] D. Youla, J. J. Bongiorno, and H. Jabr, "Modern wiener–hopf design of optimal controllers part i: The single-input-output case," *IEEE Trans. Autom. Control*, vol. 21, no. 1, pp. 3–13, 1976.

[21] V. Kucera, "Stability of discrete linear feedback systems," in *Proc. 6th IFAC World Congress, paper 44.1*, vol. 1, 1975.

[22] I. D. Landau, R. Lozano, and M. M'Saad, *Adaptive Control*, J. W. Modestino, A. Fettweis, J. L. Massey, M. Thoma, E. D. Sontag, and B. W. Dickinson, Eds. Springer-Verlag New York, Inc., 1998.

[23] B.-F. Wu and E. Jonckheere, "A simplified approach to bode's theorem for continuous-time and discrete-time systems," *IEEE Trans. Autom. Control*, vol. 37, no. 11, pp. 1797–1802, Nov 1992.

[24] IEEJ, Technical Commitee for Novel Nanoscale Servo Control, "NSS benchmark problem of hard disk drive systems," http://mizugaki.iis.u-tokyo.ac.jp/nss/, 2007.